

Chiral phase transition and thermal Hall effect in an anisotropic spin model on the kagome lattice

F. A. Gómez Albarracín,^{1,2,*} H. D. Rosales,^{1,2,†} and P. Pujol^{3,‡}

¹*Instituto de Física de Líquidos y Sistemas Biológicos (IFLYSIB), UNLP-CONICET, La Plata, Argentina and Departamento de Física, Facultad de Ciencias Exactas, Universidad Nacional de La Plata, c.c. 16, suc. 4, 1900 La Plata, Argentina*

²*Departamento de Ciencias Básicas, Facultad de Ingeniería, UNLP, 1900 La Plata, Argentina*

³*Laboratoire de Physique Théorique–IRSAMC, CNRS and Université de Toulouse, UPS, Toulouse, F-31062, France*



(Received 14 September 2020; revised 23 December 2020; accepted 21 January 2021; published 2 February 2021)

We present a study of the thermal Hall effect in the extended Heisenberg model with XXZ anisotropy in the kagome lattice. This model has the particularity that, in the classical case, and for a broad region in parameter space, an external magnetic field induces a chiral symmetry breaking: the ground state is a doubly degenerate $q = 0$ order with either positive or negative net chirality. Here, we focus on the effect of this chiral phase transition in the thermal Hall conductivity using linear-spin-waves theory. We explore the topology and calculate the Chern numbers of the magnonic bands, obtaining a variety of topological phase transitions. We also compute the magnonic effect to the critical temperature associated with the chiral phase transition (T_c^{SW}). Our main result is that, the thermal Hall conductivity, which is null for $T > T_c^{SW}$, becomes nonzero as a consequence of the spontaneous chiral symmetry breaking at low temperatures. Therefore, we present a simple model where it is possible to “switch” on/off the thermal transport properties introducing a magnetic field and heating or cooling the system.

DOI: [10.1103/PhysRevB.103.054405](https://doi.org/10.1103/PhysRevB.103.054405)

I. INTRODUCTION

One of the most significant current discussions in condensed matter physics concerns the connection between nontrivial topological properties and transport phenomena in insulating magnets [1]. It has been at the heart of numerous experimental and theoretical studies, mainly because these types of materials are candidates for carriers of the spin information without dissipation from Joule heating but with good transport coherence. Recently, particular attention has been brought upon the magnon thermal Hall effect (THE) [2–6], where the transverse heat current induced by introducing a longitudinal thermal gradient is carried by magnonic excitations.

The magnon THE was predicted theoretically and observed experimentally in materials such as the insulating ferromagnet $\text{Lu}_2\text{V}_2\text{O}_7$ [3], which has a pyrochlore lattice and antisymmetric Dzyaloshinskii-Moriya (DM) interactions perpendicular to the vanadium bonds. Other ferromagnetic pyrochlore insulators include $\text{Ho}_2\text{V}_2\text{O}_7$ and $\text{In}_2\text{Mn}_2\text{O}_7$ [7]. It has also been measured in perovskites $\text{La}_2\text{NiMnO}_6$ and YTlO [7] and kagome magnets $\text{Cu}(1-3, \text{ bdc})$ [8], $[\text{CaCu}_3(\text{OH})_6\text{Cl}_2 \cdot 0.6\text{H}_2\text{O}]$ [9]. Magnon transport has also been theoretically studied in different topological structures and models [10–16], which include both chiral and coplanar [17,18] systems. Furthermore, this transport phenomena has even led to the proposition of devices to manipulate the spin-wave current in what is called “topological magnonics” [19].

In a previous work (Ref. [20]), we presented an extended XXZ antiferromagnetic model in the kagome lattice with an emergent “spontaneous” Chern insulator, where the net chirality can be controlled by an external magnetic field. There is a hidden phase transition in terms of the scalar chirality that separates the high-temperature phase from the chiral low-temperature phase holding two $q = 0$ ground states with opposite net scalar chirality. In this paper, we explore the consequences of this chiral phase transition in the thermal Hall conductivity. Using the linear-spin-waves (LSW) theory approach, we first calculate the Chern numbers of the magnonic bands, and show that there are several topological phase transitions induced by the microscopic parameters. Then, we calculate the scalar chirality obtained from LSW and compute the the magnonic effect to the classical critical temperature. Finally, we present the effects of the chiral phase transition and the associated symmetry breaking in the thermal conductivity: a null contribution for $T > T_c^{SW}$. We close with Discussion and Conclusions.

II. MODEL AND NONINTERACTING MAGNONS

We consider the extended antiferromagnetic Heisenberg model in the kagome lattice up to third nearest-neighbor interactions, taking only third nearest-neighbors interactions across the hexagons (see Fig. 1).

$$H = \sum_{n=1}^3 \sum_{\langle i,j \rangle_n} J_n (S_i^x S_j^x + S_i^y S_j^y + \Delta S_i^z S_j^z) - h \sum_i S_i^z, \quad (1)$$

where n indicates the n th nearest neighbor, $\Delta < 1$ is the XXZ anisotropy parameter, and h is the external magnetic field

*Corresponding author. albarrac@fisica.unlp.edu.ar

†rosales@fisica.unlp.edu.ar

‡pierre.pujol@irsamc.ups-tlse.fr

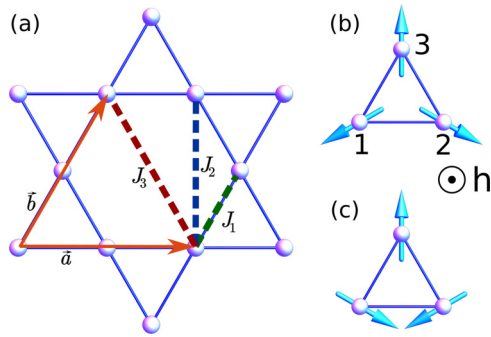


FIG. 1. (a) The kagome lattice with Bravais vectors $\vec{a} = (1, 0)$ and $\vec{b} = (\frac{1}{2}, \frac{\sqrt{3}}{2})$. First, second, and third nearest-neighbor exchange couplings, J_1 , J_2 , and J_3 , respectively, are indicated. We only consider J_3 as indicated in the figure. (b),(c) Two possible plaquette arrangements of the canted 120° ground state.

along the z direction. In the $SO(3)$ invariant $\Delta = 1$ case, the classical $T = 0$ phase diagram of this model is well known: it presents the so-called “cuboc” phases (with spontaneous and alternate scalar chirality), and a $q = 0$ phase [21,22] for $J_3 < J_2 < J_1$. At the special line $J_2 = J_3 < J_1$, the ground state has a semiextensive degeneracy [21] where lines of spins from the $q = 0$ order can be “swapped.” For practical reasons, we will take $J_1 = 1$ for the rest of the paper.

The combination of the XXZ anisotropy and an external magnetic field induces a $q = 0$ “umbrella” order with spontaneous nonzero net chirality. The emergence of scalar chirality in this simple model is quite remarkable, with a rich potential for unconventional phenomena. The xy projections of these two possible plaquette orders with opposite scalar chirality are shown in Figs. 1(b) and 1(c), where the three spins have the same projection along the field.

In these two possible ground states, the classical order is a canted 120° plaquette. The state shown in Fig. 1(b) can be described (minus a global rotation around the z axis) as $\vec{S}_1 = S(-\frac{\sqrt{3}}{2} \sin \theta, -\frac{1}{2} \sin \theta, \cos \theta)$, $\vec{S}_2 = S(\frac{\sqrt{3}}{2} \sin \theta, -\frac{1}{2} \sin \theta, \cos \theta)$, and $\vec{S}_3 = S(0, \sin \theta, \cos \theta)$ where S is the spin length and θ is the angle measured from the z axis. As is well known, the scalar chirality in a plaquette is defined as the triple product of the three spins $\chi_\Delta^0 = \vec{S}_1 \cdot (\vec{S}_2 \times \vec{S}_3)$, which is a measure of the solid angle formed by them ($\chi_\Delta^0 = S^3 3/2\sqrt{3} \cos \theta \sin^2 \theta$ for this configuration).

In a recent work [20], we focused on the special case $J_1 = 1, J_2 = 1/2, J_3 = 0, \Delta = 0.9$ and showed that at low temperature the system undergoes a phase transition where the lattice-only reflection symmetry $(x, y) \rightarrow (x, -y)$ is spontaneously broken. As discussed in Ref. [21], this symmetry transforms $\chi_{\Delta, \nabla} \rightarrow -\chi_{\nabla, \Delta}$. Therefore, the relevant order parameter is in fact the total scalar chirality (per plaquette) $\chi_{\text{tot}} = \frac{1}{N} \sum_{\Delta} \chi_{\Delta}^0$ where the sum involves all the triangular plaquettes N_{Δ} . This will allow us to study the effect of magnons in the critical temperature, defining the chirality operator, as we will show later.

In order to introduce quantum spin fluctuations and characterize the transport properties of the magnon excitations of this model, we resort to a LSW analysis [23]. Following

the standard approach, we employ a three sublattice Holstein-Primakoff (HP) mapping with the bosonic operators (see the Appendix for details).

Even though classically, there are only two types of solutions with opposite chirality, there is a rich phenomenology in the magnon spectrum. To characterize the bands of the spectrum, we calculate the Chern number C_n for each n th band, defined as $C_n = \frac{1}{2\pi} \int_{\text{BZ}} \Omega_n^z(\mathbf{k}) dk^2$, where $\Omega_n^z(\mathbf{k})$ is the Berry curvature, $\Omega_n^z(\mathbf{k}) = i \langle \frac{\partial u_n}{\partial \mathbf{k}} | \times | \frac{\partial u_n}{\partial \mathbf{k}} \rangle$, and $|u_n(\mathbf{k})\rangle$ are the Bloch waves in the n th band. To calculate this quantity numerically, we resorted to the efficient method detailed in Ref. [24], taking up to $10\,000 \times 10\,000$ points in the discretized Brillouin zone (BZ). As we describe in the next section, depending on the microscopic parameters, even for small modifications of the classical solution, the associated magnonic bands present different C_n , which leads to several interesting phenomena.

A. Topological magnonic bands and topological phase transitions

In order to discuss the magnon band structure, we choose as the classical ground state one of the two $q = 0$ states, shown in Fig. 1(b). The magnon spectrum obtained from the LSW expansion is the same for both states, but the bands have opposite C_n . From a general analysis, setting, for example, $h/S \sim 0.6$ ($\theta \sim 1.5$), we find that there are regions in the parameter space (J_2, J_3, Δ) with topologically nontrivial band structure with different C_n . These regions are divided by topological transitions that occur when the magnon bands touch, and the “local” gap between them closes. For a representative case of this situation we fix $J_2 = 0.8$ and $J_3 = 0.2$ with $\Delta \in [0, 0.9]$. The band structure for $\Delta = 0.7$ is depicted in Fig. 2(a), where there are local gaps between all the bands; $\epsilon_{\mathbf{k}, \alpha}$ indicates the energy of the $\alpha = 1, 2, 3$ band.

In Fig. 2(b) we plot the Chern number of each band as a function of Δ . Since in the $\Delta \rightarrow 1$ limit the classical ground state is degenerate, we plot up to $\Delta = 0.9$, to ensure an optimal numerical calculation of C_n . The C_n appear as steps in the constructed curve, and there are at least four topological transitions at different values of the anisotropy parameter. The sets of C_n [from the lowest ($\epsilon_{\mathbf{k}, 1}$) to the top ($\epsilon_{\mathbf{k}, 3}$) band] go as $(-3, 3, 0) \rightarrow (3, -3, 0) \rightarrow (5, -5, 0) \rightarrow (5, -7, 2) \rightarrow (-1, -1, 2)$. As Δ increases, the topology of the bands changes. For stronger XXZ anisotropy, the lower bands have opposite C_n and the top band has a trivial topology ($C_n = 0$). For higher $\Delta \gtrsim 0.65$ the top band gets a nontrivial C_n . In Fig. 2(c) we show the gap between successive bands as a function of Δ for specific points in the BZ. The Q^* point of the BZ mentioned in Fig. 2(c) is an incommensurate point between the K and Γ points, illustrated qualitatively in the inset of Fig. 2(a). This value depends on the parameters, such as the external field and the anisotropy parameter. As expected, there is a perfect correspondence between the values of Δ where there is a topological transition and the values of the anisotropy parameter where two of the bands touch. There is also a correspondence between the magnitude of the jumps and the number of points in the BZ where the gap closes and reopens: in this particular example, there is a ± 6 jump in the C_n when the bands touch at the six Q^* , and a ± 2 jump when they do at the $K(K')$ points.

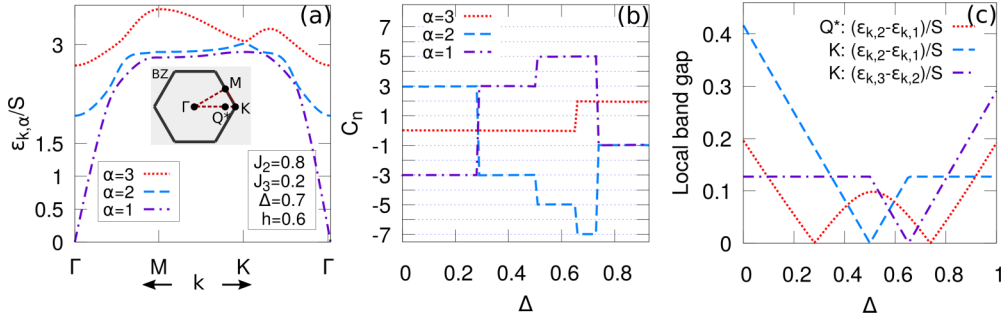


FIG. 2. Fixing $J_2 = 0.8$, $J_3 = 0.2$ (a) magnon spectrum for $h/S = 0.6$, $\Delta = 0.7$. The bands do not touch at any point in the BZ. (b) C_n for each magnon band as a function of Δ , for $\theta = 1.5$ (in radians). (c) Distance between magnon bands at different points in the BZ as a function of Δ . When the distance is zero, we identify a closing of the local gap between bands.

Another interesting issue is the role that the magnetic field plays on the topological transitions, even though classically the magnetic field just changes the canting angle of the spins. Varying the field triggers a series of topological transitions, which are reflected in the change of the C_n . We show this for $\Delta = 0.7$ in Fig. 3(a), where the C_n is $(5, -7, 2) \rightarrow (-5, 5, 0) \rightarrow (-1, 1, 0) \rightarrow (-7, 7, 0) \rightarrow (-1, 1, 0) \rightarrow (5, -5, 0)$. Since the classical saturation value is $h/S = 8.52$ (as calculated according to Eq. (A3) from the Appendix), we here plot up to $h/S = 8.5$. The $(-5, 5, 0)$ inter-

mediate region in the $(5, -7, 2) \rightarrow (-5, 5, 0) \rightarrow (-1, 1, 0)$ transition at low fields, highlighted in Fig. 3(a), is particularly narrow, and we zoom in this area in Fig. 3(b). As above, the surprisingly large values of the obtained C_n are also remarkable. A similar feature was discussed in Ref. [17], where this was attributed to an in-plane DM interaction. In our work, there are no antisymmetric interactions; the distinctive feature is the XXZ anisotropy and the antiferromagnetic nature of the couplings.

B. Chirality and phase transition

A key question in this work is the effect of magnons in the classical phase transition and the consequences on the thermal transport properties. The relevant order parameter in this case, since both ground states have the same canting angle, is not the magnetization but the scalar chirality, which allows the detection of the spontaneous symmetry breaking at low temperature. To this end, we compute the quantum version of the scalar chirality χ_{tot} using HP transformation and retaining terms up to quadratic order, obtaining

$$\langle \chi_{tot} \rangle = \left(1 + \frac{3}{2S} \right) \chi_{\Delta}^0 + \frac{S^2}{N_{\mathbf{k}}} \sum_{\mathbf{k}, \alpha=1}^3 \{ \tilde{Q}_{\mathbf{k}}^{\alpha\alpha} g(\epsilon_{\mathbf{k}, \alpha}) + \tilde{Q}_{\mathbf{k}}^{\alpha+3, \alpha+3} [1 + g(\epsilon_{\mathbf{k}, \alpha})] \}, \quad (2)$$

where $N_{\mathbf{k}}$ is the number of points in the Brillouin zone, $\chi_{\Delta}^0 = S^3 \frac{3\sqrt{3}}{2} \cos \theta \sin^2 \theta$ is the classical scalar chirality for one triangular plaquette, $g(\epsilon_{\mathbf{k}, \alpha})$ is the Bose-Einstein distribution, and $\tilde{Q}_{\mathbf{k}}$ is the chirality operator matrix in the diagonal basis (explicit expressions in the Appendix).

Let us first explore the dependence of critical temperature T_c^{SW} in terms of the spin length S taking $J_2 = 0.8$, $J_3 = 0.2$, $\Delta = 0.7h/J_1 = 0.6$. From Fig. 4(a), where we plot $\langle \chi_{tot} \rangle / S^3$ as a function of T/S^2 for different values of spin S , we observe that the chiral phase is stable up to the point $\langle \chi_{tot} \rangle / S^3 = 0$ which defines the critical temperature T_c^{SW} for each S . Looking at the $\langle \chi_{tot} \rangle / S^3$ vs T/S^2 curves for different values of S , it is clear that for a larger S there is a smaller T_c^{SW}/S^2 . Moreover, for the largest values of S , the curves tend to collapse around $T_c^{SW}/S^2 \sim 0.34$. We show $\langle \chi_{tot} \rangle / S^3$ for $S = 1$ as a function of temperature for different values of Δ [fixing $\theta = 1.5$; Fig. 4(b)] and external magnetic field [fixing $\Delta = 0.7$; Fig. 4(c)], where we can see that the behavior is robust. The

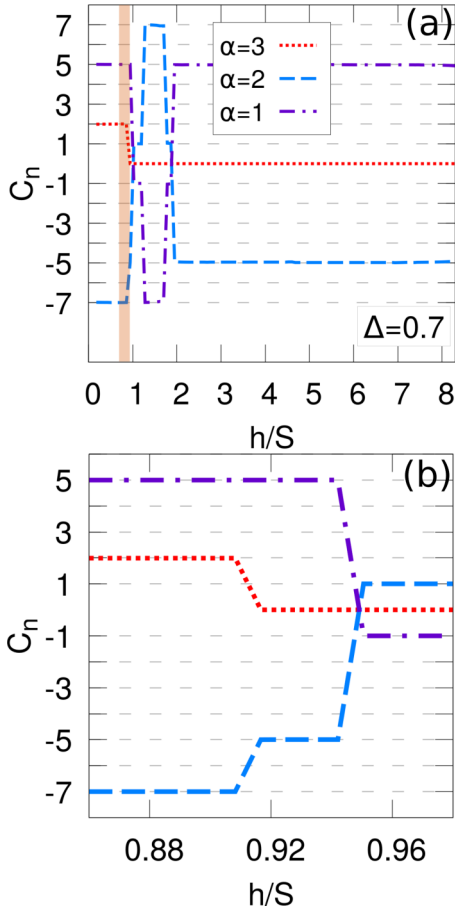


FIG. 3. Fixing $J_2 = 0.8$, $J_3 = 0.2$, $\Delta = 0.7$ (a) C_n as a function of the external magnetic field h/S . (b) Details of the highlighted area from panel (a).

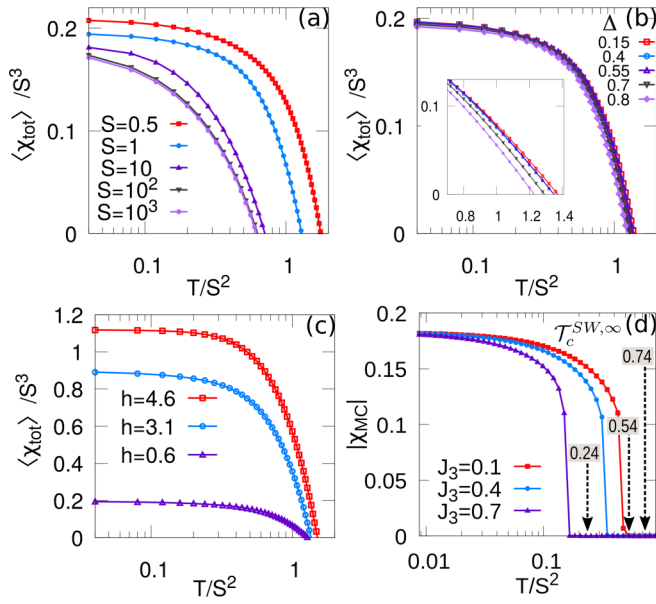


FIG. 4. Absolute value of the chirality parameter as a function of temperature from LSW for $J_2 = 0.8$, $J_3 = 0.2$ and (a) $\Delta = 0.7$, $h/S = 0.6$ and different values of S ; (b) $S = 1$, $\theta = 1.5$ and five values of Δ ; the inset zooms in to show that for higher Δ , T_c^{SW} is lower; (c) $S = 1$, $\Delta = 0.7$ and three values of h . (d) $|\chi_{\Delta}|$ vs temperature from MC simulations, $J_2 = 0.8$, $\Delta = 0.7$, $h/S = 0.6$, and $J_3 = 0.1, 0.4, 0.7$. Vertical black arrows indicate the critical temperature $T_c^{SW, \infty}$ obtained in the classical limit $S \rightarrow \infty$. Calculations were done for a discretization of $10\,000 \times 10\,000$ points in the BZ.

inset in Fig 4(b) shows that the critical temperature is lowered as the anisotropy parameter increases.

By Eq. (2), we can compute in the classical limit $T_c^{SW, \infty} = \lim_{S \rightarrow \infty} T_c^{SW}/S^2$, defined by the condition $\langle \chi_{tot} \rangle = 0$. After a simple analysis (see Appendix for details) we obtain

$$T_c^{SW, \infty} = -\frac{2\chi_{\Delta}^0}{S^3} \left[\frac{1}{N_{\mathbf{k}}} \sum_{\mathbf{k}} \sum_{\alpha=1,2,3} \frac{\tilde{Q}_{\mathbf{k}}^{\alpha\alpha} + \tilde{Q}_{\mathbf{k}}^{\alpha+3, \alpha+3}}{\omega_{\mathbf{k}, \alpha}} \right]^{-1}, \quad (3)$$

where $2S\omega_{\mathbf{k}, \alpha} = \epsilon_{\mathbf{k}, \alpha}$. Equation (3) allows us to compare $T_c^{SW, \infty}$ with Monte Carlo (MC) simulations in Fig. 4(c), as the system approaches the $J_2 = J_3$ line, where the classical model has a semiextensive degeneracy. For the MC simulations, we resort to the Metropolis algorithm combined with overrelaxation (microcanonical) updates in system size of $3L^2$ sites ($L = 30$). The estimated $T_c^{SW, \infty}$, even within the LSW approximation, seems to be of the same order of magnitude as the one obtained from MC, a situation which contrasts with three-dimensional systems with long-range magnetic order, and for which in general LSW gives a huge overestimation of the critical temperature [25]. The reason for the good estimation of the critical temperature with LSW is likely to rely on the low value (compared to the microscopic parameters) of it, implying a low contribution of the terms proportional to S^2 in Eq. (2). The most important feature of our results is that lowering the temperature from the paramagnetic phase, the quantum version of the model in Eq. (1) undergoes a phase transition in which the reflection symmetry is spontaneously broken. This has relevant consequences in the transport

properties and the thermal Hall conductivity, which we will discuss below.

C. Spontaneous thermal Hall conductivity

The presence of a nontrivial Berry curvature in the magnon bands implies the existence of a thermal Hall signature provided that the Berry curvature is not odd in momentum. The thermal Hall conductivity κ_{xy} may be calculated as [26,27]

$$\kappa_{xy} = -\frac{k_B^2 T}{(2\pi)^2 \hbar} \sum_n \int_{BZ} \left\{ c_2[g(\epsilon_{\mathbf{k}, \alpha})] - \frac{\pi^2}{3} \right\} \Omega_n^z(\vec{k}) d^2 k, \quad (4)$$

where k_B is the Boltzmann constant, $g(\epsilon_{\mathbf{k}, \alpha})$ is the Bose-Einstein distribution, and c_2 is defined as

$$c_2(x) = (1+x) \left[\ln \left(\frac{1+x}{x} \right) \right]^2 - (\ln x)^2 - 2\text{Li}_2(-x), \quad (5)$$

where $\text{Li}_2(x)$ is the dilogarithm.

In Fig. 5(a) we show κ_{xy} as a function of the external field for two temperatures $T < T_c^{SW}$. In Fig. 5(b) we show κ_{xy} [in units of $k_B^2/(2\pi\hbar)$] for $S = 1$ as a function of the temperature for different Δ , corresponding to different regions marked by the topological transitions in Fig. 2(b).

The most important feature of this study is shown in Fig. 5(c). This figure shows that the sign of κ_{xy} depends on the sign of the scalar chirality from the classical ground state. This suggests that κ_{xy} will have a spontaneous sign for $T < T_c^{SW}$. However, because $\langle \chi_{tot} \rangle = 0$ for $T > T_c^{SW}$, κ_{xy} must vanish for $T > T_c^{SW}$, implying a “switchable” THE. Unfortunately, this suppression of the κ_{xy} is not completely captured by LSW. We expect magnon interactions [25,28], not included at this stage, to establish the cancellation of κ_{xy} for $T > T_c^{SW}$. This requires a higher order spin-wave calculation (in powers of $1/S$) which is beyond the scope of this paper. Nonetheless, given the previous discussion, we propose a cutoff in κ_{xy} as represented in Fig. 5(c) with a dashed black line.

III. DISCUSSION AND CONCLUSIONS

The purpose of the present work was to study a chiral phase transition in an anisotropic Heisenberg model in the kagome lattice, in which the reflection symmetry is spontaneously broken, and where the low temperature phase shows a thermal Hall effect.

To this end, using the linear-spin-waves theory approach, we have studied numerically the topology of the magnonic bands and their Chern numbers. We have shown that there are several topological transitions driven by the magnetic field and the microscopic parameters. We have also studied the effect of magnons in the chiral phase transition in terms of these parameters. We have paid particular attention to the dependence of the critical temperature with the magnitude of the spins and obtained an interesting result comparing the value obtained taking the classical limit ($S \rightarrow \infty$) with Monte Carlo simulations.

Finally, we calculate the thermal Hall conductivity as a function of temperature showing that effectively its sign is “spontaneous.” Therefore, we show with this simple model that it is possible to “switch” on the thermal transport properties by manipulation of the external parameters.

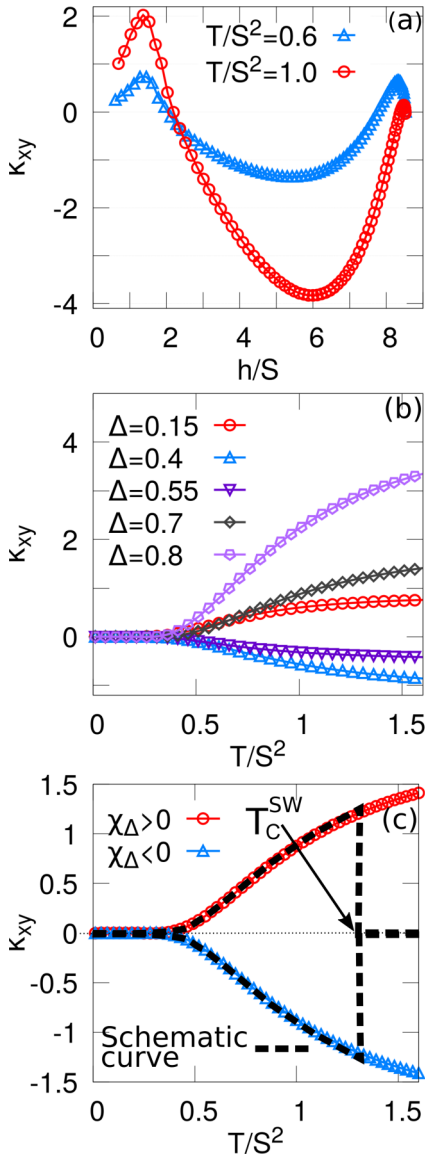


FIG. 5. For $S = 1$, $J_2 = 0.8$, $J_3 = 0.2$ (a) κ_{xy} as a function of h taking $\Delta = 0.7$ for two different temperatures $T = 0.6$ and $T = 1$; (b) thermal conductivity κ_{xy} as a function of temperature for different values of Δ , for $\theta = 1.5$; (c) κ_{xy} as a function of temperature obtained from the magnon spectrum of the two possible classical ground states with opposite scalar chirality for $\Delta = 0.7$, $h/S = 0.6$.

A unique feature of this work resides in the chiral phase transition. Previous works have established that a nonzero scalar chirality in the ground state could lead to THE. Here, the chirality serves as an order parameter associated with a spontaneous broken symmetry, and thus allows us to conjecture the behavior of the thermal Hall conductivity with temperature and define a critical temperature above which the thermal Hall conductivity is suppressed. In addition, we have shown that this conductivity can be tuned by the external magnetic field and the XXZ anisotropy. We would like to point out the fact that, although the structure of the kagome lattice allows for Dzyaloshinskii-Moriya interactions, there is still room for systems in which a spontaneously broken symmetry chiral phase as the one observed here is present (see

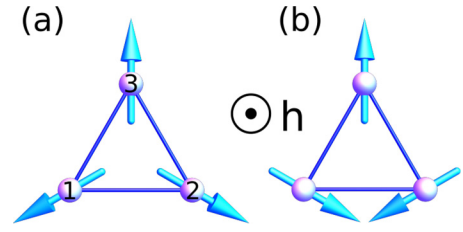


FIG. 6. Classical configuration for one plaquette: with (a) positive and (b) negative scalar chirality. The numbers 1, 2, and 3 indicate spins from the three different triangular sublattices from the kagome lattice.

Ref. [21] for a more complicated example). In this sense the example studied here has to be thought of as the simplest of a family of systems presenting a low temperature phase with a spontaneous THE.

Following the previous discussion, it would be interesting to consider magnon interactions going beyond LSW theory including three and four bosonic terms to obtain a more accurate estimation of the conductivity near the chiral phase transition. We defer this for future investigations.

ACKNOWLEDGMENTS

We would like to thank the ‘‘Laboratoire International Associ e’’ LIA LICOQ for support and Mike Zhitomirsky for very fruitful discussions. H.D.R. and F.A.G.A. acknowledge the Laboratoire de Physique Th eorique (LPT) in Toulouse for their hospitality during their 2019 visits. H.D.R. and F.A.G.A. are partially supported by PIP 2015-0813 CONICET and SECYT-UNLP. H.D.R. acknowledges support from PICT 2016-4083 and F.A.G.A. from PICT 2018-02968.

APPENDIX: SPIN-WAVE THEORY

1. Quadratic bosonic Hamiltonian and magnonic spectrum

We consider a kagome-lattice antiferromagnet with anisotropic XXZ exchange interactions up to third nearest neighbors, taking only third nearest-neighbors interactions across the hexagons. First we write the Hamiltonian as

$$H = \sum_{n=1}^3 \sum_{\langle i,\alpha;j,\beta \rangle_n} J_n (S_{i,\alpha}^x S_{j,\beta}^x + S_{i,\alpha}^y S_{j,\beta}^y + \Delta S_{i,\alpha}^z S_{j,\beta}^z) - h \sum_{i,\alpha} S_{i,\alpha}^z, \quad (\text{A1})$$

where i and j are indices for the positions \mathbf{r}_i , \mathbf{r}_j in the periodic Bravais lattice, α and β are sublattice indices (1, 2, or 3 as indicated in Fig. 6), n indicates the n th nearest neighbor, $\Delta < 1$ is the XXZ anisotropy parameter, and h is the external magnetic field along the z direction. For $J_3 < J_2 < J_1$ and $h > 0$, the classical ground state corresponds to spins forming an umbrella $q = 0$ order with spontaneous nonzero net chirality and two possible xy projections, shown in Fig. 6. The classical

energy per plaquette is given by

$$\frac{\mathcal{E}_0}{N_\Delta} = \frac{S^2}{2} [6(2J_1 + 2J_2 + J_3)\Delta \cos^2 \theta - 6(J_1 + J_2 - J_3)\sin^2 \theta] - 3hS \cos \theta, \quad (\text{A2})$$

where N_Δ is the total number of plaquettes, and θ is the canting angle between the spins and the magnetic field. Minimization of the classical energy fixes θ to

$$h = S[(2 + 4\Delta)(J_1 + J_2) + 2J_3(\Delta - 1)] \cos \theta. \quad (\text{A3})$$

In order to include quantum spin fluctuations about the classical magnetic order [Fig. 6(a) or 6(b)], we construct the Hamiltonian of free spin waves using the Holstein-Primakoff (HP) transformation [23]. We follow the conventional strategy of the large- S approach, we consider three sublattices, indicated in Fig. 6(a), and define a local coordinate system along the direction of the classical ground state as spin quantization axis $\{x'_n, y'_n, z'_n\}$. The HP transformation in the local frame reads

$$\tilde{S}_{i,\alpha}^z = S - a_{i,\alpha}^\dagger a_{i,\alpha}, \quad (\text{A4})$$

$$\tilde{S}_{i,\alpha}^+ = \sqrt{2S - a_{i,\alpha}^\dagger a_{i,\alpha}} a_{i,\alpha} \approx a_{i,\alpha} \sqrt{2S}, \quad (\text{A5})$$

$$\tilde{S}_{i,\alpha}^- = a_{i,\alpha}^\dagger \sqrt{2S - a_{i,\alpha}^\dagger a_{i,\alpha}} \approx a_{i,\alpha}^\dagger \sqrt{2S} \quad (\text{A6})$$

with $a_{i,\alpha}^\dagger$ ($a_{i,\alpha}$) being a bosonic creation (annihilation) operator of the sublattice α at the cell i . Using this mapping in the Hamiltonian given by Eq. (A1) and after a Fourier transformation $a_{i,\alpha} = (1/\sqrt{N}) \sum_{\mathbf{k}} e^{i\mathbf{k}\cdot(\mathbf{r}_i + \mathbf{r}_\alpha)} a_{\mathbf{k},\alpha}$, where N is the total number of unit cells, \mathbf{r} denotes the position of the unit cell and \mathbf{r}_α are the internal positions of the sublattices. The bilinear bosonic Hamiltonian reads

$$H_2 = S \sum_{\mathbf{k}} \Psi_{\mathbf{k}}^\dagger \cdot M_{\mathbf{k}} \cdot \Psi_{\mathbf{k}}, \quad (\text{A7})$$

where $\Psi_{\mathbf{k}}^\dagger = \{a_{\mathbf{k},1}^\dagger, a_{\mathbf{k},2}^\dagger, a_{\mathbf{k},3}^\dagger, a_{-\mathbf{k},1}, a_{-\mathbf{k},2}, a_{-\mathbf{k},3}\}$ and the matrix $M_{\mathbf{k}}$ is

$$M_{\mathbf{k}} = \begin{bmatrix} D_{\mathbf{k}} & C_{\mathbf{k}} \\ C_{\mathbf{k}}^\dagger & D_{-\mathbf{k}}^T \end{bmatrix}, \quad (\text{A8})$$

where the submatrix $D_{\mathbf{k}}, C_{\mathbf{k}}$ has elements

$$\begin{aligned} D_{\mathbf{k}}^{11} &= \frac{1}{2} \{h/S c\theta - 2c\theta^2 \Delta(2J_1 + 2J_2 + J_3) + 2(J_1 + J_2 - J_3)s\theta^2 + J_3(1 + c\theta^2 + \Delta s\theta^2) \cos[2(q_1 - q_2)]\}, \\ D_{\mathbf{k}}^{21} &= -\frac{1}{8}(3 + c2\theta + 4i\sqrt{3}c\theta - 2\Delta + 2c2\theta \Delta)[J_1 \cos(q_1) + J_2 \cos(q_1 - 2q_2)], \\ D_{\mathbf{k}}^{31} &= \frac{1}{4}(-1 + 2i\sqrt{3}c\theta - c\theta^2 + 2\Delta s\theta^2)[J_2 \cos(2q_1 - q_2) + J_1 \cos(q_2)], \\ D_{\mathbf{k}}^{12} &= -\frac{1}{8}(3 + c2\theta - 4i\sqrt{3}c\theta - 2\Delta + 2c2\theta \Delta)[J_1 \cos(q_1) + J_2 \cos(q_1 - 2q_2)], \\ D_{\mathbf{k}}^{22} &= \frac{1}{2} [h/S c\theta - 2c\theta^2 \Delta(2J_1 + 2J_2 + J_3) + 2(J_1 + J_2 - J_3)s\theta^2 + J_3(1 + c\theta^2 + \Delta s\theta^2) \cos(2q_2)], \\ D_{\mathbf{k}}^{32} &= \frac{1}{4}(-1 - 2i\sqrt{3}c\theta - c\theta^2 + 2\Delta s\theta^2)[J_1 \cos(q_1 - q_2) + J_2 \cos(q_1 + q_2)], \\ D_{\mathbf{k}}^{13} &= \frac{1}{4}(-1 - 2i\sqrt{3}c\theta - c\theta^2 + 2\Delta s\theta^2)[J_2 \cos(2q_1 - q_2) + J_1 \cos(q_2)], \\ D_{\mathbf{k}}^{23} &= \frac{1}{4}(-1 + 2i\sqrt{3}c\theta - c\theta^2 + 2\Delta s\theta^2)[J_1 \cos(q_1 - q_2) + J_2 \cos(q_1 + q_2)], \\ D_{\mathbf{k}}^{33} &= \frac{1}{2} [h/S c\theta - 2c\theta^2 \Delta(2J_1 + 2J_2 + J_3) + 2(J_1 + J_2 - J_3)s\theta^2 + J_3(1 + c\theta^2 + \Delta s\theta^2) \cos(2q_1)], \end{aligned}$$

$$\begin{aligned} C_{\mathbf{k}}^{11} &= \frac{1}{2}(-1 + \Delta)J_3 s\theta^2 \cos[2(q_1 - q_2)], \\ C_{\mathbf{k}}^{21} &= \frac{1}{4}(1 + 2\Delta)s\theta^2 [J_1 \cos(q_1) + J_2 \cos(q_1 - 2q_2)], \\ C_{\mathbf{k}}^{31} &= \frac{1}{4}(1 + 2\Delta)s\theta^2 [J_2 \cos(2q_1 - q_2) + J_1 \cos(q_2)], \\ C_{\mathbf{k}}^{12} &= \frac{1}{4}(1 + 2\Delta)s\theta^2 [J_1 \cos(q_1) + J_2 \cos(q_1 - 2q_2)], \\ C_{\mathbf{k}}^{22} &= \frac{1}{2}(-1 + \Delta)J_3 s\theta^2 \cos(2q_2), \\ C_{\mathbf{k}}^{32} &= \frac{1}{4}(1 + 2\Delta)s\theta^2 [J_1 \cos(q_1 - q_2) + J_2 \cos(q_1 + q_2)], \\ C_{\mathbf{k}}^{13} &= \frac{1}{4}(1 + 2\Delta)s\theta^2 [J_2 \cos(2q_1 - q_2) + J_1 \cos(q_2)], \\ C_{\mathbf{k}}^{23} &= \frac{1}{4}(1 + 2\Delta)s\theta^2 [J_1 \cos(q_1 - q_2) + J_2 \cos(q_1 + q_2)], \\ C_{\mathbf{k}}^{33} &= \frac{1}{2}(-1 + \Delta)J_3 s\theta^2 \cos(2q_1), \end{aligned}$$

where we have defined $q_1 = k_x$, $q_2 = k_x/2 + \sqrt{3}/2k_y$, $s\theta = \sin \theta$, $c\theta = \cos \theta$, $s2\theta = \sin 2\theta$, and $c2\theta = \cos 2\theta$.

To diagonalize the bosonic Hamiltonian we perform a paraunitary Bogoliubov transformation [29] $M_d = U_{\mathbf{k}}^\dagger \cdot M_{\mathbf{k}} \cdot$

$U_{\mathbf{k}} = \text{diag}\{w_{\mathbf{k},1}, w_{\mathbf{k},2}, w_{\mathbf{k},3}, w_{-\mathbf{k},1}, w_{-\mathbf{k},2}, w_{-\mathbf{k},3}\}$ with $U_{\mathbf{k}}^\dagger \cdot \sigma_3 \cdot U_{\mathbf{k}} = \sigma_3$, $\sigma_3 = \text{diag}\{1, 1, 1, -1, -1, -1\}$. The bilinear Hamiltonian becomes

$$H_{eff} = \mathcal{E}_0 + \sum_{\mathbf{k},\alpha} \epsilon_{\mathbf{k},\alpha} \left(b_{\mathbf{k},\alpha}^\dagger b_{\mathbf{k},\alpha} + \frac{1}{2} \right), \quad (\text{A9})$$

where the energy of the magnon bands is $\epsilon_{\mathbf{k},\alpha} = 2S\omega_{\mathbf{k},\alpha}$ [28].

2. Chirality order parameter

Following the same strategy, we perform the HP transformation [Eq. (A4)] in the chirality operator $\chi_{tot} = \frac{1}{N_\Delta} \sum_{\Delta} \chi_{\Delta}$, with $\chi_{\Delta} = \mathbf{S}_i \cdot (\mathbf{S}_j \times \mathbf{S}_k)$. Retaining up to quadratic bosonic terms, we obtain

$$\begin{aligned} \langle \chi_{tot} \rangle &= \left(S^3 + \frac{3}{2} S^2 \right) \frac{3\sqrt{3}}{2} \cos \theta \sin^2 \theta \\ &+ \frac{S^2}{N_{\mathbf{k}}} \sum_{\mathbf{k}\alpha=1}^3 \left\{ \tilde{Q}_{\mathbf{k}}^{\alpha\alpha} g(\epsilon_{\mathbf{k},\alpha}) + \tilde{Q}_{\mathbf{k}}^{\alpha+3,\alpha+3} [1 + g(\epsilon_{\mathbf{k},\alpha})] \right\}, \end{aligned} \quad (\text{A10})$$

where $N_{\mathbf{k}}$ is the number of points in the Brillouin zone, $g(\epsilon_{\mathbf{k},\alpha})$ is the Bose-Einstein distribution, and $\tilde{Q}_{\mathbf{k}} = U_{\mathbf{k}}^\dagger \cdot Q \cdot U_{\mathbf{k}}$ with

$$Q = \begin{bmatrix} -B & A & A^* & 0 & -\frac{B}{2} & -\frac{B}{2} \\ A^* & -B & A & -\frac{B}{2} & 0 & -\frac{B}{2} \\ A & A^* & -B & -\frac{B}{2} & -\frac{B}{2} & 0 \\ 0 & -\frac{B}{2} & -\frac{B}{2} & -B & A^* & A \\ -\frac{B}{2} & 0 & -\frac{B}{2} & A & -B & A^* \\ -\frac{B}{2} & -\frac{B}{2} & 0 & A^* & A & -B \end{bmatrix} \quad (\text{A11})$$

with $A = \frac{1}{32}(8i + 5\sqrt{3} \cos \theta + 3\sqrt{3} \cos 3\theta)$ and $B = \frac{3\sqrt{3}}{4} \cos \theta \sin^2 \theta$.

From Eq. (A10) we can obtain the value of the critical temperature in the classical limit, $\mathcal{T}_c^{SW,\infty} = \lim_{S \rightarrow \infty} T_c^{SW}/S^2$. In order to do this, we take the $S \rightarrow \infty$ limit in the Bose distribution function (setting the Boltzmann constant $k_B = 1$):

$$\begin{aligned} g(\epsilon_{\mathbf{k},\alpha}) &= g(2S\omega_{\mathbf{k},\alpha}) = \frac{1}{\exp^{2S\omega_{\mathbf{k},\alpha}/T} - 1} \\ &= \frac{1}{\exp^{(2\omega_{\mathbf{k},\alpha}/S)(1/T/S^2)} - 1} \implies \lim_{S \rightarrow \infty} g(2S\omega_{\mathbf{k},\alpha}) \\ &\sim \frac{1}{1 + \frac{2\omega_{\mathbf{k},\alpha}}{S} \frac{1}{T/S^2} + \dots - 1} = \frac{S\mathcal{T}_c^{SW,\infty}}{2\omega_{\mathbf{k},\alpha}}. \end{aligned} \quad (\text{A12})$$

Inserting the above expression for $g(\epsilon_{\mathbf{k},\alpha})$ in Eq. (A10) and taking $\langle \chi_{tot} \rangle = 0$ we obtain the expression for $\mathcal{T}_c^{SW,\infty}$ shown in Eq. (3) in the main text.

-
- [1] Y. Tokura, K. Yasuda, and A. Tsukazaki, *Nat. Rev. Phys.* **1**, 126 (2019).
- [2] H. Katsura, N. Nagaosa, and P. A. Lee, *Phys. Rev. Lett.* **104**, 066403 (2010).
- [3] Y. Onose, T. Ideue, H. Katsura, Y. Shiomi, N. Nagaosa, and Y. Tokura, *Science* **329**, 297 (2010).
- [4] R. Matsumoto and S. Murakami, *Phys. Rev. Lett.* **106**, 197202 (2011).
- [5] R. Matsumoto and S. Murakami, *Phys. Rev. B* **84**, 184406 (2011).
- [6] S. Murakami and A. Okamoto, *J. Phys. Soc. Jpn.* **86**, 011010 (2017).
- [7] T. Ideue, Y. Onose, H. Katsura, Y. Shiomi, S. Ishiwata, N. Nagaosa, and Y. Tokura, *Phys. Rev. B* **85**, 134411 (2012).
- [8] M. Hirschberger, R. Chisnell, Y. S. Lee, and N. P. Ong, *Phys. Rev. Lett.* **115**, 106603 (2015); R. Chisnell, J. S. Helton, D. E. Freedman, D. K. Singh, R. I. Bewley, D. G. Nocera, and Y. S. Lee, *ibid.* **115**, 147201 (2015).
- [9] H. Doki, M. Akazawa, H. Y. Lee, J. H. Han, K. Sugii, M. Shimozawa, N. Kawashima, M. Oda, H. Yoshida, and M. Yamashita, *Phys. Rev. Lett.* **121**, 097203 (2018).
- [10] P. Laurell and G. A. Fiete, *Phys. Rev. Lett.* **118**, 177201 (2017).
- [11] A. Mook, J. Henk, and I. Mertig, *Phys. Rev. B* **90**, 024412 (2014).
- [12] A. Mook, J. Henk, and I. Mertig, *Phys. Rev. B* **91**, 224411 (2015).
- [13] S. A. Owerre, *Phys. Rev. B* **95**, 014422 (2017).
- [14] X. S. Wang, Ying Su, and X. R. Wang, *Phys. Rev. B* **95**, 014435 (2017).
- [15] K. Hwang, N. Trivedi, and M. Randeria, *Phys. Rev. Lett.* **125**, 047203 (2020).
- [16] M. Kawano and C. Hotta, *Phys. Rev. B* **99**, 054422 (2019).
- [17] P. Laurell and G. A. Fiete, *Phys. Rev. B* **98**, 094419 (2018).
- [18] A. Mook, J. Henk, and I. Mertig, *Phys. Rev. B* **99**, 014427 (2019).
- [19] X. S. Wang, H. W. Zhang, and X. R. Wang, *Phys. Rev. Appl.* **9**, 024029 (2018).
- [20] H. D. Rosales, F. A. Gómez Albarracín, and P. Pujol, *Phys. Rev. B* **99**, 035163 (2019).
- [21] F. A. Gómez Albarracín and P. Pujol, *Phys. Rev. B* **97**, 104419 (2018).
- [22] L. Messio, C. Lhuillier, and G. Misguich, *Phys. Rev. B* **83**, 184401 (2011).
- [23] A. Auerbach, *Interacting Electrons and Quantum Magnetism* (Springer-Verlag, New York, 1994).
- [24] T. Fukui, Y. Hatsugai, and H. Suzuki, *J. Phys. Soc. Jpn.* **74**, 1674 (2005).
- [25] Z. Li, T. Cao, and S. G. Louie, *J. Magn. Magn. Mater.* **463**, 28 (2018).
- [26] R. Matsumoto, R. Shindou, and S. Murakami, *Phys. Rev. B* **89**, 054420 (2014).
- [27] A. Mook, J. Henk, and I. Mertig, *Phys. Rev. B* **89**, 134409 (2014).
- [28] A. L. Chernyshev and M. E. Zhitomirsky, *Phys. Rev. Lett.* **113**, 237202 (2014); *Phys. Rev. B* **79**, 144416 (2009); **91**, 219905(E) (2015).
- [29] J. Colpa, *Phys. A: Stat. Mech. Appl.* **93**, 327 (1978).